12-3-2010

Measurements of Gas-Phase Inorganic and Organic Acids from Biomass Fires by Negative-Ion Proton-Transfer Chemical-Ionization Mass Spectrometry

P. Veres
University of Colorado at Boulder

James M. Roberts
NOAA Earth System Research Laboratory

I. R. Burling
University of Montana - Missoula

C. Warneke
University of Colorado at Boulder

Joost de Gouw
University of Colorado at Boulder

See next page for additional authors

Follow this and additional works at: https://scholarworks.umt.edu/chem_pubs

Part of the Biochemistry Commons, and the Chemistry Commons

Let us know how access to this document benefits you.

Recommended Citation

Veres, P., J. M. Roberts, I. R. Burling, C. Warneke, J. de Gouw, and R. J. Yokelson (2010), Measurements of gasphase inorganic and organic acids from biomass fires by negative-ion proton-transfer chemical-ionization mass spectrometry, J. Geophys. Res., 115, D23302, doi:10.1029/2010JD014033.

Authors

P. Veres, James M. Roberts, I. R. Burling, C. Warneke, Joost de Gouw, and Robert J. Yokelson

Measurements of gas-phase inorganic and organic acids from biomass fires by negative-ion proton-transfer chemical-ionization mass spectrometry

Patrick Veres,[1,2] James M. Roberts,[2] Ian R. Burling,[3] Carsten Warneke,[2,4] Joost de Gouw,[2,4] and Robert J. Yokelson[3]

[1]   Emissions from 34 laboratory biomass fires were investigated at the combustion facility of the U.S. Department of Agriculture Fire Sciences Laboratory in Missoula, Montana. Gas-phase organic and inorganic acids were quantified using negative-ion proton-transfer chemical-ionization mass spectrometry (NI-PT-CIMS), open-path Fourier transform infrared spectroscopy (OP-FTIR), and proton-transfer-reaction mass spectrometry (PTR-MS). NI-PT-CIMS is a novel technique that measures the mass-to-charge ratio (m/z) of ions generated from reactions of acetate ($CH_3C(O)O^-$) ions with inorganic and organic acids. The emission ratios for various important reactive acids with respect to CO were determined. Emission ratios for isocyanic acid (HNCO), 1,2 and 1,3-benzenediols (catechol, resorcinol), nitrous acid (HONO), acrylic acid, methacrylic acid, propionic acid, formic acid, pyruvic acid, and glycolic acid were measured from biomass burning. Our measurements show that there is a significant amount of HONO in fresh smoke. The NI-PT-CIMS measurements were validated by comparison with OP-FTIR measurements of HONO and formic acid (HCOOH) and with PTR-MS measurements of HCOOH.

1.   Introduction

[2]   Biomass burning is a significant source of atmospheric gases and particles. It occurs naturally in wildfires and is also employed by over half the world population for cooking, land clearing, heating, lighting, and other uses [*Crutzen and Andreae*, 1990]. In the United States, prescribed fires are widely used to accomplish many beneficial land management objectives such as reducing the danger of larger, more destructive wildfires [*Mutch*, 1994]. Biomass burning emissions strongly affect regional air quality, and can also be transported over large distances to impact regions distant from the source [*Bytnerowicz et al.*, 2009; *Warneke et al.*, 2009]. Characterization of smoke emissions produced by the wide range of fuels commonly burned must be performed to understand and manage the effects of bio-

mass burning emissions on regional-global atmospheric chemistry. The most abundant compounds emitted to the atmosphere by biomass burning are water vapor, carbon dioxide (CO_2), and carbon monoxide (CO); however, there are thousands of additional compounds emitted in smoke plumes. Previous studies have shown that oxygenated volatile organic compounds (OVOCs) account for most of the nonmethane organic carbon (NMOC) released from biomass fires [*Christian et al.*, 2004; *Karl et al.*, 2007; *Yokelson et al.*, 1996, 1997]. Many of these compounds remain poorly characterized due to analytical challenges. As a result, the individual contributions to the total OVOC component of biomass emissions are poorly understood. Measurements of this class of compounds are needed to accurately set initial photochemical model conditions that assess the local and long-range transport effects of smoke.

[3]   One poorly understood, but significant class of OVOCs present in biomass burning smoke is gas-phase organic acids [*de Gouw et al.*, 2006; *Yokelson et al.*, 2008]. Previous work has shown that the formation of both secondary organic aerosol (SOA) and organic acids in urban plumes is more rapid than box models can explain [*de Gouw et al.*, 2005; *Grieshop et al.*, 2009; *Volkamer et al.*, 2006]. In addition, analysis by aerosol mass spectrometry (AMS) suggests that a significant fraction of SOA consists of organic acids [*Takegawa et al.*, 2007]. These two observa-

[1]Department of Chemistry and Biochemistry, University of Colorado at Boulder, Colorado, USA.
[2]Chemical Sciences Division, Earth System Research Laboratory, National Oceanic and Atmospheric Administration, Boulder, Colorado, USA.
[3]Department of Chemistry, University of Montana, Missoula, Montana, USA.
[4]Cooperative Institute for Research in Environmental Sciences, University of Colorado at Boulder, Boulder, Colorado, USA.

Table 1. Fires and Fuel Type Sorted by Region

Fire Name	Number of Fires	Fuel Description	Origin
Ceanothus	1	Ceanothus	Fort Hunter-Liggett
Manzanita	5	Manzanita	Vandenburg Air Force Base (AFB)
CA Sage	4	California Sagebrush-Artemisia, Ericameria	Vandenburg AFB
Coastal Sage	2	Coastal Sage Scrub-Salvia Mellifera, Artemisia, Ericameria	Vandenburg AFB
Maritime Chaparral	2	Maritime Chaparral-Ceanothus Cuneatus, Ericameria spp, UNKN app, Salvia mellifera, grass, Ceanothus spp.	Vandenburg AFB
Oak Savannah	2	Emory Oak Savanna-Quercus Emoryl, Erogrostis Lehmanni	Fort Huachuca
Oak Woodland	2	Emory Oak Woodland-Quercus Emoryl Pointleaf Manzanita, Leaf Litter	Fort Huachuca
Mesquite	3	Masticated Mesquite-Prosopis Velutina Desert Broom-Baccharis Sarthoydes	Fort Huachuca
1 yr Rough NC	3	1 year Rough	North Carolina
2 yr Rough NC	3	2 year Rough	North Carolina
Treated NC	2	Treated	North Carolina
Untreated NC	3	Untreated	North Carolina
Pocosin	3	Pocosin	North Carolina
Pine Litter	3	Pine Litter, Duff	Fort Benning

tions suggest that organic acids could be intimately involved with SOA formation and, therefore, that direct emission of organic acids from biomass burning could represent a significant source of precursors for SOA [*Carlton et al.*, 2006; *Walser et al.*, 2007]. Unfortunately, however most gas-phase organic acids have been extremely difficult to measure because of their adsorptive nature and a lack of sufficiently selective instrumentation.

[4] The development of chemical-ionization mass spectrometry techniques has been essential to our understanding of the chemical composition of various air masses [*Huey*, 2007; *Viggiano*, 1993]. Specifically, negative-ion chemical-ionization mass spectrometry techniques (NI-CIMS) have improved our ability to measure many atmospherically relevant species [*Amelynck et al.*, 2000; *Custer et al.*, 2000; *Viidanoja et al.*, 1998, 2000]. Recently, the development of negative-ion proton-transfer chemical-ionization mass spectrometry (NI-PT-CIMS) has improved the prospects for measuring acidic species [*Veres et al.*, 2008]. An opportunity to sample biomass burning smoke with NI-PT-CIMS was presented in February of 2009 at the combustion facility of the U.S. Department of Agriculture (USDA) Fire Sciences Laboratory (FSL) in Missoula, Montana, to obtain better information about the atmospheric impacts associated with prescribed burning in various ecosystems of the southwest and southeast United States. In the course of this work the NI-PT-CIMS also detected significant emissions of several important inorganic acids such as nitrous acid (HONO) and isocyanic acid (HNCO). We present the emission ratios of nine important gas-phase acids to CO measured during 34 biomass fires burned in the combustion facility of the Missoula Fire Sciences Laboratory. Atmospheric implications of the measurements will be discussed, including the potential of the measured organic acids to contribute to SOA formation and of the measured HONO to affect OH levels in biomass burning plumes. In this paper, we present a validation of our NI-PT-CIMS measurements through a direct comparison to open-path Fourier transform infrared

spectroscopy (FTIR) measurements of both formic acid and HONO.

2. Experimental Details

2.1. Combustion Facility

[5] The combustion facility at the U.S. Department of Agriculture (USDA) Forest Service, Fire Sciences Laboratory (FSL) in Missoula, Montana, has a large burn chamber (12.5 m × 12.5 m × 22 m high). Fuels are burned on a ~2 m^2 bed below a 1.6 m diameter exhaust stack with a 3.6 m inverted funnel opening [*Christian et al.*, 2003; *McMeeking et al.*, 2009]. The room is pressurized with temperature and humidity conditioned air, which is vented through the stack, completely entraining any emissions from the fires. A sampling platform surrounds the stack, at a height of 17 m, and the temperature, pressure, trace-gas, and particle measurement equipment was installed here except for a PTR-MS and a Gas Chromatography Mass Spectrometer (GC-MS) that were located in an adjacent observation room. Previous work has shown that fire emissions are well mixed in the stack at the height of the sampling platform [*Christian et al.*, 2004]. Residence times in the stack ranged from 5 to 17 s throughout the measurement period [*Burling et al.*, 2010].

2.2. Biomass Fuels

[6] Table 1 summarizes information on each type of fuel burned. Fuels were collected to represent regional vegetation from the southwestern United States and southeastern United States. Fuels collected from both regions were shipped to the FSL and carefully reassembled in the facility based on photographs and mass/acre measurements.

[7] The southwestern fuels were chosen to accurately reflect the predominant vegetation at two California facilities managed by the Department of Defense (DoD) (Vandenberg AFB and Fort Hunter-Liggett). Approximately 5.7 million hectares (17%) of California's vegetation is classified as brush with a significant percentage known as the shrub complex chaparral. Chaparral is a significant com-
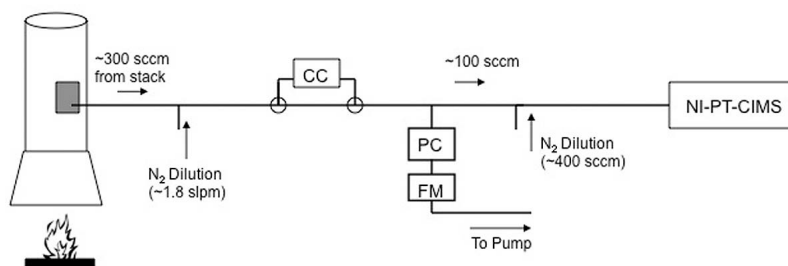
Figure 1. Schematic diagram of the NI-PT-CIMS inlet used during the Firelab study. Air is sampled from the smoke stack (~300 cm^3 min^{-1} STP) through a 1/8″ (0.32 cm) Teflon line and diluted using dry N$_2$. A pressure controller (PC) and flowmeter (FM) are used in series to control the last 0.3 m of the inlet to a pressure of ~400 mbar. Approximately 100 cm^3 min^{-1} STP of dilute stack flow is mixed with ~400 cm^3 min^{-1} STP dry N$_2$ in a secondary dilution stage. A catalytic converter (CC) can be switched in line to provide instrument backgrounds. The entire length of the inlet is controlled to 80°C.

ponent of the vegetation at the DoD facilities listed above. Several common species comprise the bulk of plants and were selected as the predominant southwestern biomass fuels for this study: chamise (*Adenostoma fasciculatum*), ceanothus (*Ceanothus spp.*), manzanita (*Arctostaphylos spp.*), and scrub oak (*Quercus berberidifolia*). Fuels from the southeastern U.S. were collected from Camp Lejeune in North Carolina and Fort Benning in Georgia. The ecosystems found at Camp Lejeune are good proxies for the ecosystems that dominate DoD bases throughout the southeastern U.S. Two examples of typical vegetation communities present in this region are (1) a low live fuel component comprised of long-leaf pine savanna community dominated by oak, wire grass, pine needle litter, and dead woody fuel, and (2) high or tall pocosin shrub-dominated, a significant live fuel component, leaf litter, and duff.

2.3. NI-PT-CIMS Measurements

2.3.1. Principle of the NI-PT-CIMS Measurement

[8] NI-PT-CIMS provides gas-phase acid measurements with one-second time resolution. The fast time response and high sensitivity of NI-PT-CIMS make it ideal for measurements of both organic and inorganic acids in rapidly changing conditions such as these biomass burning experiments. A detailed description of NI-PT-CIMS can be found elsewhere [*Veres et al.*, 2008]. Briefly, NI-PT-CIMS consists of (1) a ^{210}Po source to produce acetate ions (CH$_3$C(O)O$^-$) from acetic anhydride, (2) a flow tube reactor (40 mbar), in which CH$_3$C(O)O$^-$ undergoes proton transfer reactions with inorganic and organic acids in ambient air, (3) a collisional dissociation chamber (CDC) (0.2 mbar) to fragment cluster ions, and (4) a linear quadrupole mass spectrometer for the detection of both reagent and product ions.

[9] Acetate ions react with organic and inorganic acids (HA) in the flow tube by the following reaction:

$$CH_3C(O)O^- + HA \rightarrow CH_3C(O)OH + A^-. \quad (1)$$
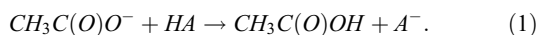
Acids with gas-phase acidity higher than that of acetic acid will undergo the above reaction. Gas-phase acidity is defined as the Gibbs free energy change of the following reaction:

$$HA \rightarrow H^+ + A^-. \quad (2)$$

In addition to reaction (1), the A$^-$ and CH$_3$COO$^-$ ions can cluster with water molecules and other neutrals that are sampled in air. The presence of these ion clusters serves to complicate the acquired mass spectra making interpretation difficult. Cluster ion formation is effectively reduced in the CDC where a high electric field (25 V cm^{-1}) and pressure (0.2 mbar) are applied to collisionally dissociate weakly bound cluster ions, such as CH$_3$C(O)O$^-$•(H$_2$O)$_n$, into their core ions. Evidence of cluster ions in the mass spectra is absent with the exception of m/z 119, CH$_3$C(O)OH• CH$_3$C(O)O$^-$.

[10] We can use the following kinetic equations to determine the expected concentration (or count rate) of A$^-$:

$$[CH_3C(O)O^-]_{\Delta t} = [CH_3C(O)O^-]_0 \times e^{-k[HA]t} \quad (3)$$

$$[A^-]_t = [CH_3C(O)O^-]_0 \times \left[1 - e^{-k[HA]t}\right], \quad (4)$$

where [A$^-$] and [CH$_3$COO$^-$] are measured ion counts of the conjugate base and generated acetate ions respectively, [HA] is the concentration of trace gas HA, k is the rate of the proton abstraction reaction detailed in equation (1) and t the reaction time. If k[HA]t is small, i.e., only a small fraction of CH$_3$COO$^-$ ions react in the flow tube, equation (4) simplifies to the following:

$$[A^-]_t = [CH_3C(O)O^-]_0 \times k[HA]t. \quad (5)$$

Although in theory equation (5) can be used to calculate gas-phase concentrations, in practice, calibrations based on laboratory-generated standards were used in this study. Gas-phase concentrations can be calculated using sensitivities measured from laboratory standards as follows:

$$[HA] = \frac{[A^-]}{CF_{Acid} \times [CH_3C(O)O^-]} \times 10^6, \quad (6)$$

where CF$_{Acid}$ is the calibrated sensitivity (normalized to 10^6 reagent ion counts) for the acid being measured. Ion signals are normalized to remove any influence of the changing concentration of acetate ions.

2.3.2. Gas Inlet System

[11] The NI-PT-CIMS sampled biomass burning emissions through a bulkhead plate on the combustion stack at

Table 2. Calibration Source Types, Uncertainties, and Instrumental Detection Limits

	Calibration Source Type	Calibration Method	Source Error (%)	Effective Detection Limit[a] (ppb)	Instrumental Detection Limit[b] (ppb)
Methacrylic	Diffusion Cell	MOCCS[c]	15	0.7	0.01
Pyruvic/Butyric	Diffusion Cell	MOCCS	15	0.4	0.02
HCOOH	Permeation Source	MOCCS	10	2.5	0.13
Glycolic	Diffusion Cell	MOCCS	15	0.4	0.03
Acrylic	Diffusion Cell	MOCCS	15	0.7	0.05
Propionic	Diffusion Cell	MOCCS	15	0.4	0.02
Benzenediol	Diffusion Cell	MOCCS	15	0.6	0.11
HNCO[d]	Diffusion Cell	FTIR	10	0.7	0.10
HONO[d]	Permeation Source	NO_y Conversion	15	2.7	0.06

[a]The effective detection limit is defined as twice the standard deviation in background measurements made in the smoke stack prior to fire ignition.
[b]The instrumental detection limit is defined as twice the standard deviation in the background measured during an instrument zero using zero air.
[c]Details are given by *Veres et al.* [2010].
[d]Details of the calibration source used are given by *Roberts et al.* [2010].

the height of the sampling platform. A 1/4″ (0.64 cm) o.d. stainless steel tube was installed on the interior of the stack pointed straight up to minimize the amount of particles sampled during a fire. A 1/8″ (0.32 cm) o.d. PFA Teflon tube was inserted inside the stainless tubing and attached to the CIMS inlet on the external side of the bulkhead. The section of the CIMS inlet external to the stack is shown in Figure 1. The inlet consisted of 3 m of 1/8″ (0.32 cm) o.d. PFA Teflon tubing that was temperature controlled to 80°C. The last 0.3 m of the inlet was pressure controlled to 300 Torr.

[12] In undiluted smoke, large concentrations of reactive acids caused reductions in the acetate ion concentration of >50%, which caused the instrument response to become nonlinear. A detailed discussion of the ion kinetics in a reagent ion depleted system can be found in Appendix A. In order to reduce this effect, a multistage dilution system was designed to decrease the mixing ratio of sampled emissions in the NI-PT-CIMS. A N_2 dilution stream was added at two junctions in the main inlet line to reduce the sampled concentration by a factor of 35.

2.3.3. Calibrations

[13] Calibrations of NI-PT-CIMS were performed using the inlet shown in Figure 1 in the NOAA laboratory and at the FSL. Calibration gases were added to the front of the inlet to account for inlet losses and dilution. Most inorganic and organic acid standards for the compounds measured during the study were developed and used for calibration in the laboratory subsequent to the Fire Laboratory measurements. Table 2 contains a complete list of the species that were calibrated and the types of sources used. Also contained in Table 2 are the source calibration methods used, errors associated with each calibration method, and instrumental detection limits.

[14] Standard mixtures of inorganic acids, HONO and HNCO, were produced in real-time using sources that have been discussed elsewhere [*Roberts et al.*, 2010]. Briefly,

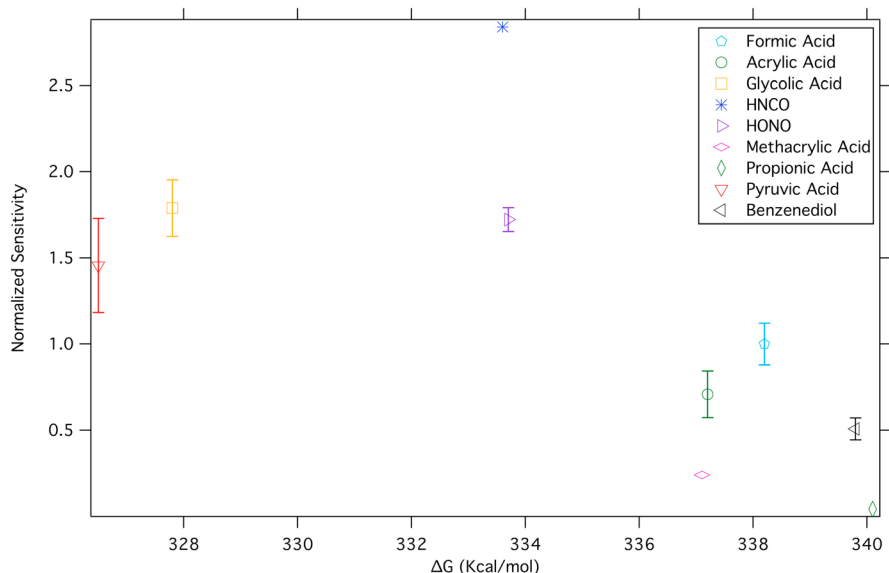**Figure 2.** Summary of organic acid calibrations normalized to formic acid graphed versus gas-phase acidity (ΔG) [*Linstrom and Mallard*, 2010]. The gas-phase acidity of acetic acid is 341.5 kcal/mol. Errors shown reflect 1 standard deviation on the average of replicate sensitivity measurements where possible. In the case where error bars are not shown, only a single calibration point was available.
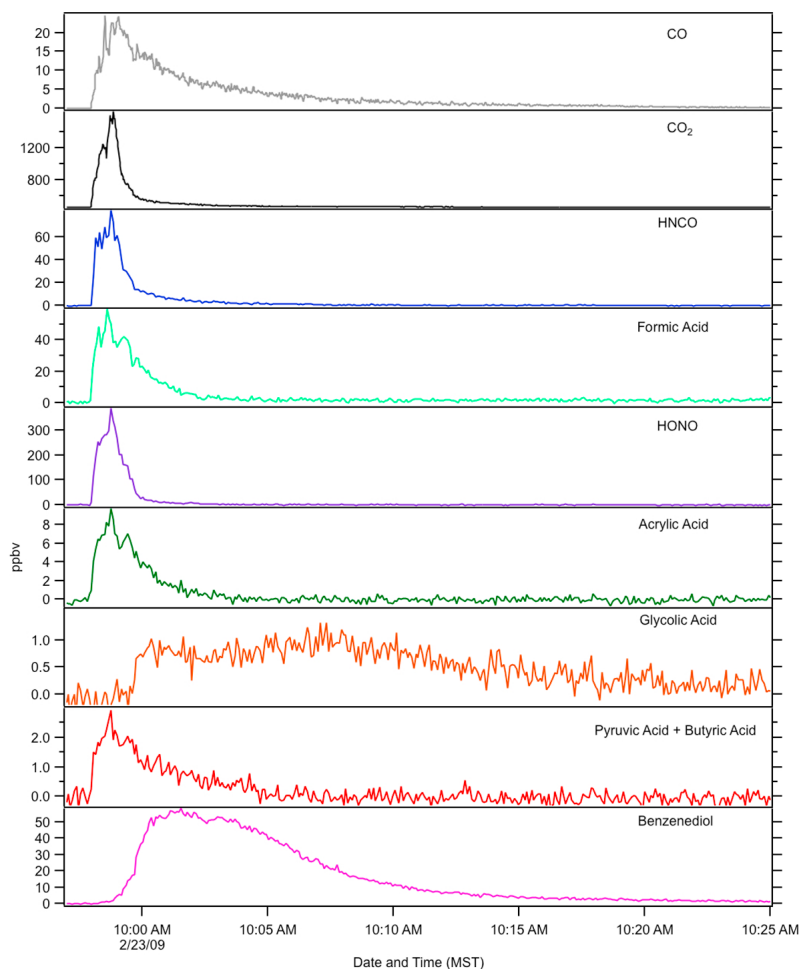
Figure 3. NI-PT-CIMS analysis of a typical laboratory fire (2 year rough North Carolina) taken in selected ion mode. The acid data shown are 1 s measurements acquired every 10 s. CO and CO_2 data are taken from OP-FTIR.

HONO was generated by flowing gaseous HCl over a bed of sodium nitrite in the presence of water vapor. Isocyanic acid was generated by heating cyanuric acid to 210°C in a glass capillary diffusion cell.

[15] Organic acid calibrations were done by passing zero air over a thermostated permeation source or through a diffusion cell containing the pure substance. The method with which these sources were calibrated is discussed elsewhere [*Veres et al.*, 2010]. In short, the organic acid standard stream, in air, is passed over a heated palladium catalyst oxidizing the acid to CO_2 with a 1:1 conversion of each carbon to CO_2. The resulting CO_2 is measured by non-dispersive infrared spectroscopy (NDIR) and the organic acid concentration can be calculated.

[16] A formic acid permeation source calibrated using the above mentioned method was used as the primary standard for field calibration of the NI-PT-CIMS response. To account for instrumental drift and changes in the dilution, multiple formic acid calibrations were performed per day, throughout the study and were constant to within ±20%. Laboratory calibration factors (CF_{acid}) for all other acids were normalized to a simultaneously measured formic acid calibration factor (CF_{formic}). These calibration ratios (F_{acid} =

CF_{acid}/CF_{formic}) were collected under relative humidity conditions ranging from 0 to 100%. Average sensitivity from replicate measurements at various relative humidity settings are shown in Figure 2 as a function of gas-phase acidity. The variability in measured sensitivities is within the calibration source error (Table 2), and as such we conclude that no significant effects of water vapor were observed.

[17] Mixing ratios were calculated using the following equation:

$$[HA] = 10^6 \times \frac{[A^-]}{[PI^-] \times F_{acid} \times CF_{HCOOH}}, \qquad (7)$$

where $[A^-]$ is the measured ion signal of the acid of interest, $[PI^-]$ the effective primary ion signal (i.e., the sum of ions that will produce A^- in reactions with HA) and CF_{HCOOH} the formic acid calibration factor measured in the field. Using this technique, any instrumental drift in sensitivity should be accounted for by normalizing to the formic acid sensitivity. Based on the variation of F_{acid} measured and taking into account the daily variation in formic acid calibrations ($CF_{HCOOH} \approx 140 \pm 20\%$ Hz ppbv^{-1}) an error of
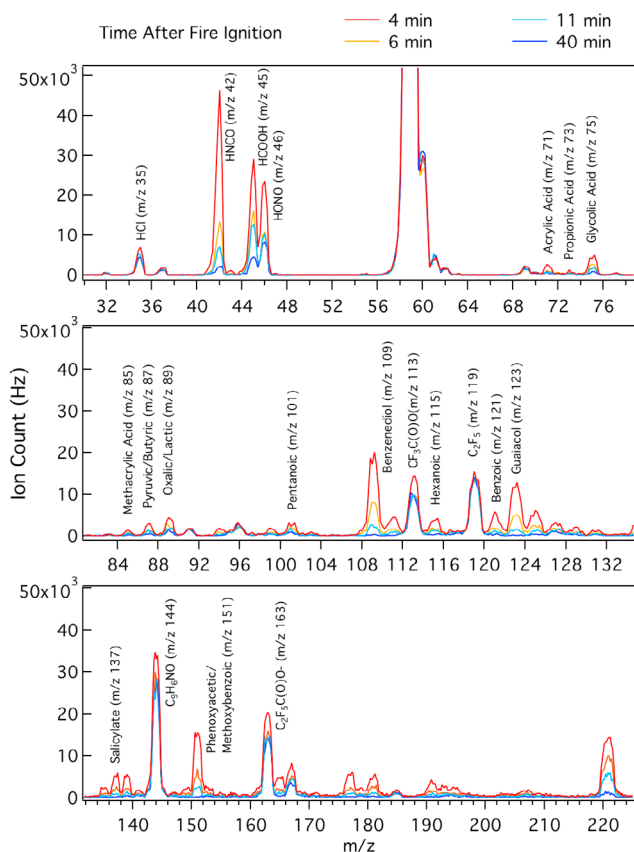
Figure 4. Successive full mass scans taken at various stages in a fire (Georgia litter) with proposed identities of the signal observed at the listed m/z ratio. Spectra have been normalized to 10^6 counts per second of m/z 59 ($CH_3C(O)O^-$).

±25% has been assigned to acid concentrations calculated using this method.

2.4. OP-FTIR

[18] The open path Fourier transform infrared (OP-FTIR) instrument included a Bruker Matrix-M IR Cube spectrometer and a thermally stable open White cell. The White cell was positioned on the sampling platform approximately 17 m above the fuel bed so that it spanned the stack directly in the rising emissions stream. The White cell path length was set to 58 m. The spectral resolution was set to 0.67 cm^{-1} and the spectrometer acquired spectra every 1.5 s (four co-added spectra) beginning several minutes prior to the fire and continuously until the end of the fire. A pressure transducer and two temperature sensors were located adjacent to the optical path and were logged on the instrument computer and used for spectral analysis.

[19] The acquired spectra were analyzed offline for CO_2, CO, H_2O, N_2O, NO_2, NO, HONO, NH_3, HCl, SO_2, CH_4, CH_3OH, HCHO, HCOOH, C_2H_2, C_2H_4, CH_3COOH, HCN, propylene and furan. Mixing ratios were obtained by multicomponent fits to sections of the IR transmission spectra with a synthetic calibration nonlinear least squares method [*Griffith*, 1996; *Yokelson et al.*, 2007a]. Excess mixing ratios

were calculated by subtraction of a 60 s average mixing ratio prior to the ignition of the fire.

2.5. PTR-MS

[20] PTR-MS utilizes proton-transfer reactions of H_3O^+ to detect various atmospheric trace gases, usually as the protonated parent (MH^+) ion. PTR-MS allows for the detection of numerous volatile organic compounds with high sensitivity (10–100 pptv) and response time (1–10 s). This technique has been used extensively in aircraft, ground-based and laboratory studies. A more complete discussion of the PTR-MS system used in this study can be found elsewhere [*de Gouw and Warneke*, 2007].

[21] During this study, a PTR-MS was located in an observation room outside the main combustion chamber. Both NI-PT-CIMS and PTR-MS sampled from the same bulkhead plate on the combustion stack. Inside the stack an upward facing inlet identical to the one described for the NI-PT-CIMS was used. The sample line consisted of approximately 20 m of unheated 1/4″ o.d. PFA Teflon with a flow of 8 standard liters per minute (sLpm). The PTR-MS subsampled (~200 cm^3 min^{-1} STP) from this main flow through 1/8″ heated PEEK tubing.

3. Results

[22] Measurements of formic acid were performed using the three techniques discussed in this study. We report NI-PT-CIMS versus OP-FTIR and NI-PT-CIMS versus PTR-MS comparisons for HCOOH measurements of all fuels where a comparison is possible. Also, NI-PT-CIMS and OP-FTIR measurements of HONO are compared when possible. Comparison of the various methods will be reported as the slope of the orthogonal distance regression. Average NI-PT-CIMS emission ratios of the various species measured to CO are also reported. Various unknown m/z ion signals observed throughout the study will be discussed and an identity suggested when appropriate.

3.1. NI-PT-CIMS Measurement Modes

[23] NI-PT-CIMS has two different modes of operation that were used during this study. The primary method that was used during the fires was selected ion mode. In selected ion mode, up to ten masses can be monitored sequentially over a period of 5 s. Figure 3 shows an example of data collected while operating in selected ion mode. Figure 3 shows the simultaneous increases in the mixing ratios of many acids during one burn, along with CO and CO_2 measured by OP-FTIR. For this particular fuel, the flaming stage (CO_2, HONO) lasted only a few minutes and the smoldering stage (CO, organic acids) less than an hour. These data are then used to calculate the emission ratios reported here. In addition to operating in this selected ion mode, several full mass spectra were taken scanning from m/z 10 to m/z 225. This was done to survey which compounds were present in the smoke. Figure 4 shows the result of several full mass scans taken throughout a given fire. The benefit of this operating mode is the ability to identify a larger number of compounds than selected ion mode allows.

[24] The selective nature of this measurement technique limits the number of possible reactive compounds yielding ions at a given m/z ratio. Gas-phase acidities can be used to
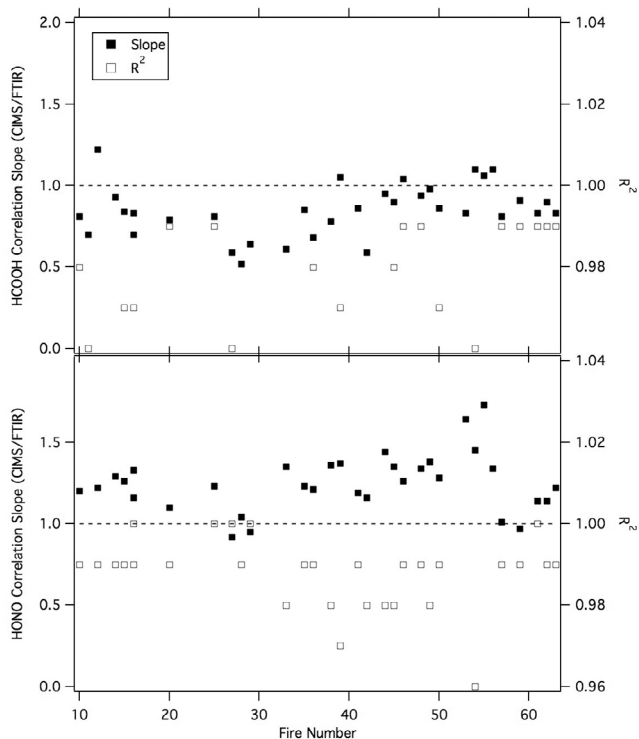
Figure 5. Summary of the NI-PT-CIMS and FTIR comparison data for all the fires reported. Data shown are the slope and R^2 value acquired from an ODR fit of FTIR and CIMS data for each fire.

limit the possible identities of unknown m/z signals. The soft nature of the ionization process limits fragmentation further simplifying the process of identification. In some cases, such as HONO that is detected as NO_2^- (m/z 46), isotopic analysis can be used to support a proposed identity. Once an identity is suggested, laboratory studies of pure standards are used to verify the appearance of the product ion at the specific m/z and quantify the instrument response.

3.2. Intercomparison of Formic Acid

[25] A comparison of NI-PT-CIMS and OP-FTIR formic acid measurements was possible for 34 of the fires sampled. Although more than 34 fires were sampled, the remainder of the fires were not included in this comparison due to data loss as a result of interruptions in the selected ion mode caused by the acquisition of full mass spectra. The results of the formic acid comparison for each individual fire are summarized in Figure 5. Figure 6a shows a correlation plot of NI-PT-CIMS/OP-FTIR formic acid measurements of the combined data for the 34 fires. The NI-PT-CIMS/OP-FTIR formic acid ratio, i.e., the slope of an orthogonal distance regression, is 0.90 ± 0.01 with a correlation (R^2) of 0.97 for the combined fire data. The agreement between these two measurements in the overall data set is well within the estimated uncertainty of both instruments.

[26] The comparison between NI-PT-CIMS to PTR-MS for the duration of the study is shown in Figure 6b. The NI-PT-CIMS/PTR-MS ratio is 1.38 ± 0.01 with a correlation (R^2) of 0.98. The underestimation of formic acid concentration by PTR-MS is probably due to inlet losses. As dis-

cussed by *Veres et al.* [2008], formic acid losses of approximately 25% were observed across an unheated 10m Teflon inlet. We attribute inlet losses to surface deposition and diffusion into the Teflon tubing although specific loss mechanisms have not been studied. Extrapolating the formic acid loss to an inlet length of 20m suggests losses of up to 44%. In a similar study, a 60% reduction in formic acid was observed in PTR-MS measurements when compared to OP-FTIR [*Christian et al.*, 2004]. Ethanol is a potential interference in the PTR-MS measurement of formic acid [*Veres et al.*, 2008]. GC-MS measurements of ethanol showed that it was present at only a few percent of formic acid. There was no good correlation between CIMS measurements of formic acid and GC-MS ethanol.

3.3. Intercomparison of HONO

[27] The results of the HONO comparison for each individual fire are summarized in Figure 7. The NI-PT-CIMS versus FTIR HONO ratio from the orthogonal distance regression, Figure 7, was 1.19 ± 0.01 with a correlation (R^2)
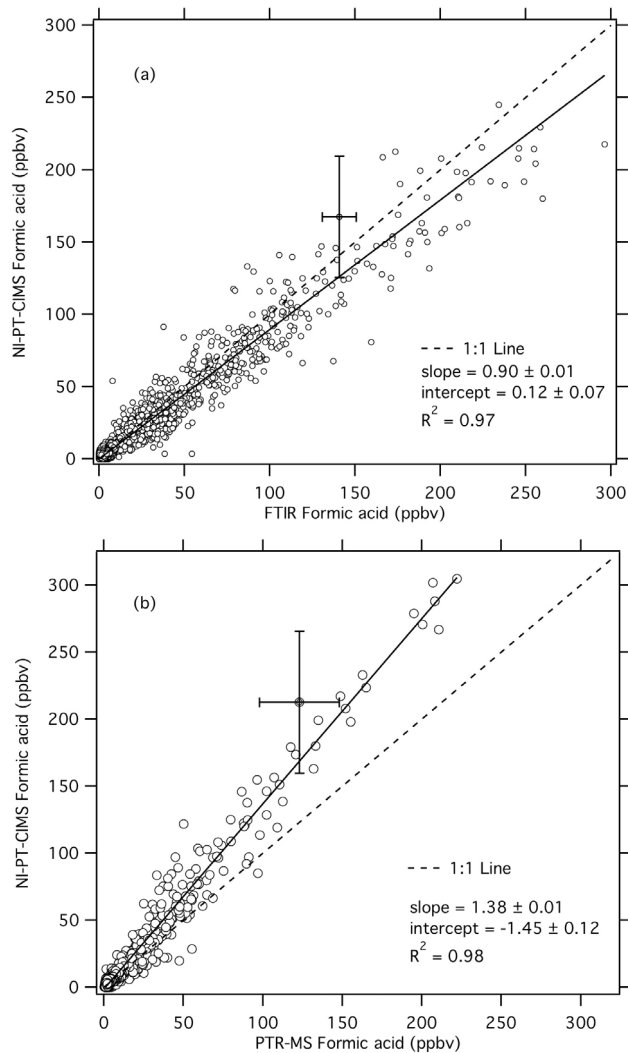

Figure 6. Comparison plot of NI-PT-CIMS to (a) FTIR and (b) PTR-MS formic acid measurements for the total combined fire data for all 34 fires sampled.
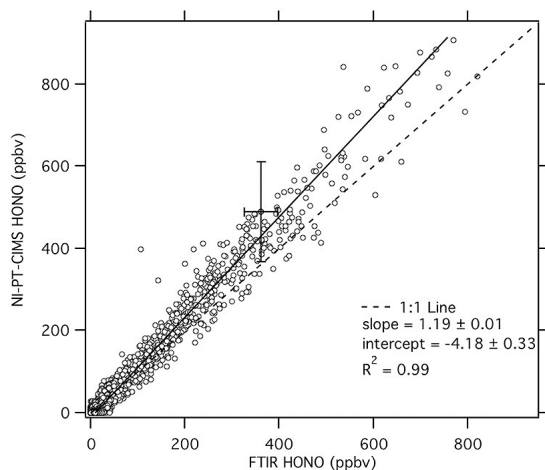
Figure 7. Comparison plot of NI-PT-CIMS and FTIR HONO measurements for the total combined fire data for every fuel type sampled.

of 0.99 for the combined data from 34 fires. Figure 7 shows a systematically higher measurement for the NI-PT-CIMS HONO in the fires, although the difference is still within the combined uncertainties. This difference could occur for one or more of the following reasons: (1) an error in the CIMS calibration factor used for HONO, (2) a potential interference in the CIMS measurement due to production of HONO in the CIMS inlet, or (3) error in the FTIR retrievals.

[28] Several potential interferences in HONO measurements have been examined [*Roberts et al.*, 2010] including decomposition of $HNO_3 \cdot NO_3^-$ clusters within the CIMS, and NO_2-water production on inlet surfaces. These potential interferences are discussed in further detail in *Roberts et al.* [2010] where they conclude from laboratory studies that these effects are quite minor (≤1%, 3.3%, respectively) at the levels observed in the fires.

3.4. Emission Ratios

[29] NI-PT-CIMS emission ratios (ER) were calculated using the method described by *Yokelson et al.* [2007b]. Emission ratios are a widely used quantity where excess mixing ratios (ΔX) are calculated relative to a simultaneously measured mixing ratio for another plume species: usually a tracer such as ΔCO. CO mixing ratios by FTIR were used to calculate emission ratios for the acids measured with NI-PT-CIMS. The acidic species measured here were not always tightly correlated with CO over the course of one fire. We obtained ratios for NI-PT-CIMS compounds with respect to CO from the integrated mixing ratios (in ppb s^{-1}) for each fuel. Table 2 shows the average molar emission ratios measured for each fuel type sampled. When possible, the data shown are averages of replicate measurements of the fuel listed. An average ER is presented for all fuels grouped by the southwestern and southeastern United States in Table 3.

3.4.1. HNCO (m/z 42$^-$)

[30] One of the highest signals during the fires was observed at 42 amu, which we attribute here to isocyanic acid (HNCO). Other possible contributors to this mass include cyanic acid, HOCN, fulminic acid, HCNO, or hydrazoic acid (N_3H) but they were discounted for reasons

detailed elsewhere [*Roberts et al.*, 2010]. An HNCO mixture in N_2 was generated in the laboratory from thermal dissociation of cyanuric acid and was indeed detected at 42 amu. HNCO is produced almost exclusively in the flaming stage, with low-level production observed during the smoldering stage. The average ER measured in the southwest fuels (0.76 mmol molCO^{-1}) is nearly identical to that observed in the southeastern fuels (0.78 mmol molCO^{-1}).

3.4.2. Formic Acid (m/z 45$^-$)

[31] Formic acid is emitted throughout the smoldering and flaming stages of a fire. The regional average ER varied from 0.34 mmol molCO^{-1} in the southwest to 1.7 mmol molCO^{-1} in the southeast fuels. Figure 8 shows a summary of the formic acid ER measured for each fuel type. Figure 8 (top right) shows a summary of previously published formic acid emission ratios from both field and laboratory measurements. The overall comparison suggests that formic acid ER are highly variable and that fuel specific measurements are valuable.

3.4.3. HONO (m/z 46$^-$)

[32] Figure 8 (bottom left) shows average HONO ER measurements for each fuel type. The ER variability between the southwestern and southeastern fuels, 0.95 mmol molCO^{-1} and 1.4 mmol molCO^{-1}, respectively, has significantly less regional average differences than that observed in the organic acid measurements. However, the fuel-average ER does vary by a factor of three for the fuel types presented. Figure 8 shows previously published measurements of HONO. The fact that the field measurements lie in the upper half of the spread in the laboratory measurements suggests that the HONO observed here is not an artifact occurring from production on the stack walls.

3.4.4. Acrylic Acid (m/z 71$^-$)

[33] The signal at 71 amu is attributed here to acrylic acid. Other possibilities for this mass include cyclopropyl carbinol and butenol but they are not likely because their gas-phase acidity is lower than that of acetic acid. Acrylic acid was emitted in both the flaming and smoldering stage with the predominant emissions observed during the flaming stage. The average ER$_{CO}$ was measured as 0.041 mmol molCO^{-1} and 0.18 mmol molCO^{-1} in the southwestern and southeastern fuels, respectively.

3.4.5. Propionic Acid (m/z 73$^-$)

[34] The signal at 73 amu is attributed here to propionic acid. Another common compound that could appear at this mass is butanol but it would not be observed in this system because its gas-phase acidity is lower than that of acetic acid. Propionic acid was only quantitatively measured during a single burn of the Manzanita fuel type. This particular

Table 3. Average Enhancement Ratios of Organic Acids to CO for Southwest and Southeast Regional Fuels[a]

	Southwest Fuels	Southeast Fuels
Methacrylic	0.04	–
Pyruvic/Butyric	0.04 ± 0.02	0.24 ± 0.16
HCOOH	0.81 ± 0.46	3.24 ± 1.72
Glycolic	0.04 ± 0.02	0.44 ± 0.33
Acrylic	0.11 ± 0.06	0.55 ± 0.31
Propionic	0.61 ± 0.02	–
Benzenedio	1 1.56 ± 1.16	17.97 ± 12.83
Total Organic Acids	3.23	22.44

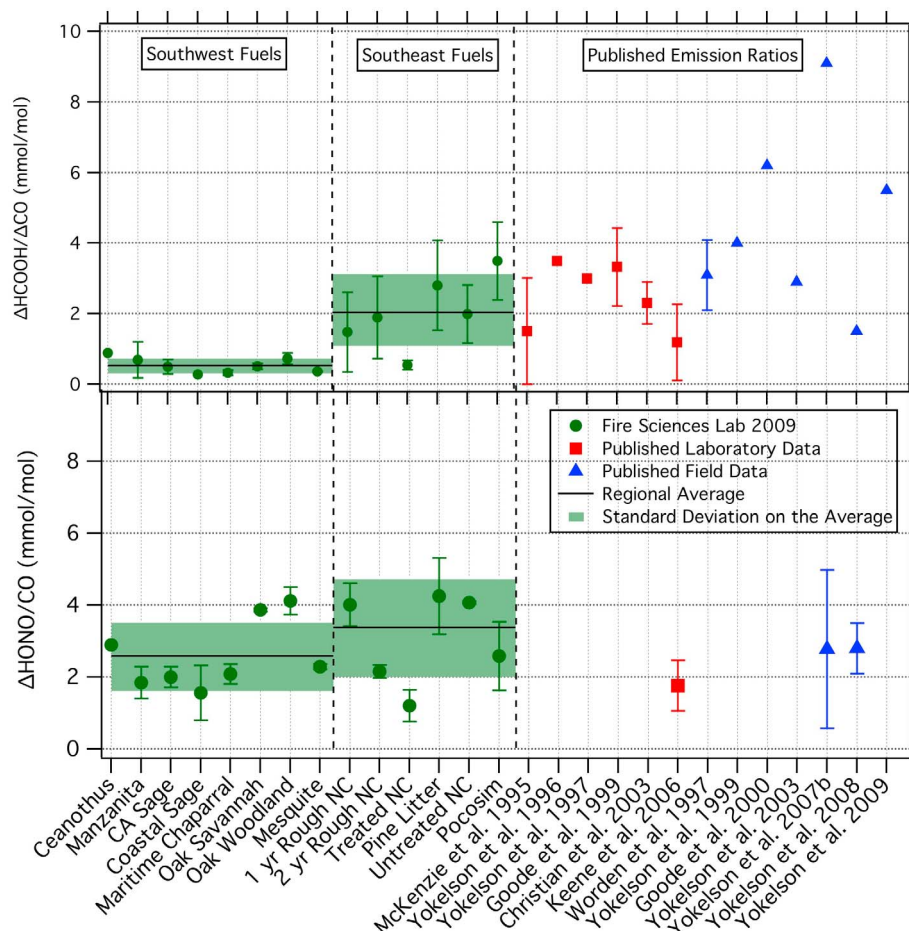[a]Ratios are reported in μg m^{-3} ppmvCO^{-1}.

Figure 8. Emission ratios of HCOOH and HONO from this study are shown on the left of the panel. The solid black line in the southwest and southeast fuels plots represents the regional average ER with 1 standard deviation on the average shown in solid green. Measured emission ratios from 13 previously published studies are shown for both HCOOH and HONO on the right for comparison. [*Christian et al.*, 2003; *Goode et al.*, 1999, 2000; *Keene et al.*, 2006; *McKenzie et al.*, 1995; *Worden et al.*, 1997; *Yokelson et al.*, 1996, 1997, 1999, 2003, 2007b, 2008, 2009]. Data from all studies except Keene and Mckenzie were rescaled to reflect the new HCOOH IR cross section [*Rothman et al.*, 2009].

m/z (73) was not monitored during the rest of the fires presented here. The calculated emission ratio was determined to be 0.203 mmol molCO^{-1}.

3.4.6. Glycolic Acid (m/z 75$^-$)

[35] The signal at 75 amu is attributed here to glycolic acid. Another possible identity is peroxyacetic acid, which cannot be ruled out, as to our knowledge the gas-phase proton affinity has not yet been measured. Glycolic acid was observed in both the flaming and smoldering stage, most strongly correlating with benzenediol. The average emission ratio measured in the southwestern fuels is 0.013 mmol molCO^{-1} and 0.13 mmol molCO^{-1} (10 times higher) in the southeastern fuels. The temporal profile of the glycolic acid emissions suggests that it may stick to the inlet somewhat, but it is released well within the period of integration over the course of the fire. Thus the ER presented should be accurate.

3.4.7. Methacrylic Acid (m/z 85$^-$)

[36] The signal at 85 amu is attributed here to methacrylic acid. Other possibilities for this mass included crotonic acid, 3-butenoic acid, cyclopropanecarboxylic acid and CF$_3$OH,

where the proton abstraction reaction of these molecules with the acetate is thermochemically favorable. The anion of crotonic acid is a possible contributor to the signal at m/z 85, however formation would likely occur through a process involving 1,3 pentadiene. In comparison to the production pathway of methacrylic acid, likely a reaction pathway involving isoprene, the contribution of crotonic acid to the m/z 85 signal is expected to be small. A similar argument can be made for the formation of 3-butenoic acid; however, contribution to m/z 85 signal cannot be overlooked for both crotonic acid and 3-butenoic acid. Cyclopropanecarboxylic acid is structurally unlikely to be formed during the smoldering phase of biomass fires where the m/z 85 signal was observed. CF$_3$OH will react to form an anion at m/z 85; however, it is unlikely to be present. The presence of perfluoro compounds in biomass smoke would be a result of environmental contaminants, as they are not found in natural biomass. To our knowledge there have not been any measurements of fluorinated compounds in biomass emissions previously, moreover there is no change in m/z 19 (F$^-$) which

would be an expected fragment if fluorinated compounds were present. Methacrylic acid was only quantitatively measured in a single fire of the fuel type Ceanothus. The emission ratio for methacrylic was 0.013 mmol molCO^{-1}.

3.4.8. Pyruvic/Butyric Acid (m/z 87$^-$)

[37] The signal at 87 amu is attributed here to the sum of pyruvic and butyric acid. Other possibilities for this mass include pentanol and methylbutanol but they are not likely because their gas-phase acidity is lower than that of acetic acid. Pyruvic acid and butyric acid will both undergo proton abstraction to form m/z 87. Using this technique it is not possible to separate these compounds so we report the data as the sum of both species. For data analysis purposes, the calibration factor for pyruvic acid was used. Pyruvic acid ($\Delta G_{equation\ 1}$ = 326.5 kcal/mol) has a lower proton affinity than butyric acid ($\Delta G_{equation\ 1}$ = 339.1 kcal/mol). Figure 2 implies that the sensitivity should be higher for pyruvic acid than butyric acid. For this reason, the values reported for this m/z should be considered a lower limit estimate of the sum of both species as concentration goes as the reciprocal of the sensitivity. The average ER measured in the southwestern and southeastern regions is 0.031 mmol molCO^{-1} and 0.061 mmol molCO^{-1}, respectively.

3.4.9. Benzenediol (m/z 109$^-$)

[38] Two isomers 1,2- and 1,3-benzenediol can undergo reaction with $CH_3C(O)O^-$ based on their gas-phase acidity. The 1,4-benzenediol isomer (hydroquinone) has a lower gas-phase acidity than acetic acid and therefore will not be detected using the NI-PT-CIMS ion chemistry. The 1,3-benzenediol isomer was used for calibration during this study. There was a significant dependence of ER on fuel region with the southeastern fuels yielding higher ER than the southwestern fuels. The average ER for southwestern fuels, 0.37 mmol molCO^{-1}, is approximately 13 times less than that observed in the southeastern fuels, 4.7 mmol molCO^{-1}.

3.4.10. Proposed Attribution of Unidentified m/z

[39] The compounds discussed above have previously been detected at the listed mass-to-charge ratios using laboratory standards. The species for which ER are reported were monitored during the duration of at least one fire in the selected ion mode. We propose the following identities to various signals frequently observed in the intermittent full mass scan spectra based on their gas-phase acidity and structure: HCl (m/z 35, 37), HNO_3 (m/z 62), oxalic acid or lactic acid (m/z 89), pentanoic acid (m/z 101), CF_3COO^- (m/z 113), hexanoic acid (m/z 115), C_2F_5 and $CH_3COOH \cdot CH_3COO^-$ (m/z 119), benzoic acid (m/z 121), guaiacol (m/z 123), salicylic (m/z 137), $C_9H_6NO^-$ (m/z 144), phenoxyacetic acid or methoxybenzoic acid (m/z 151), and $C_2F_5COO^-$ (m/z 163). The presence of fluorinated compounds is purposed to be a result of the heated Teflon inlets used in these measurements. Fluorinated ions are frequently observed in negative ion CIMS spectra from the off gassing of Teflon tubing. Of the species listed here HCl, HNO_3, and benzoic acid have all been detected at those respective masses using laboratory-generated standards. Accurate measurements of HCl and HNO_3 were not possible during this study due to inlet losses and memory effects. Although we cannot unambiguously identify the other species listed, we suggest the above as probable identities of these observed ions. Future work will be performed to expand our ability to identify these and other unknown m/z.

4. Discussion

[40] There are two well recognized stages of combustion during a fire: (1) a flaming process that converts greater than 95% of the fuel carbon to CO_2 and (2) a smoldering process that produces high CO emissions as a result of relatively inefficient combustion and only converts 60–85% of the fuel carbon to CO_2. Organic acids were observed to correlate most strongly with CO emissions throughout the fire. The long inlet response times of glycolic acid and benzenediol make it difficult to show correlation to either CO or CO_2; however, the delayed onset of these compounds during a fire suggests production by the smoldering process. This trend is apparent in Figure 3 by the late appearance of both compounds. HNCO and HONO correlate best with the CO and CO_2, respectively, produced early in the fire when it is dominated by flaming combustion.

[41] There are significant differences in the regional average ER for most of the organic compounds measured. Formic acid, glycolic acid, acrylic acid and benzenediol are 5 to 13 times larger in the southeastern fuels than the southwestern fuels. The southwestern ER was 2 times lower than the southeastern ER for m/z 87 (Pyruvic/Butyric acid). One possible source of these compounds is the pyrolysis of the lignin in the fuels burned. Large differences in lignin content of the fuels collected from each region could explain the significant variation in southwestern and southeastern ER. Inorganic acids show far less variation in the regional average ER. HONO and HNCO regional average ER differ by factors of up to 1.5.

[42] The HNCO measurements reported here are among the first observations of this compound in experiments that simulate biomass burning. Our measurements show a consistent production of HNCO by flaming combustion, most clearly correlated to flaming production of CO. Figure 9 contains a summary of HNCO to flaming production of CO ratios for all fires. It can be observed that this ratio remains relatively constant for all fuel types sampled. Hansson *et al.* [*Hansson et al.*, 2004] previously reported the formation of HNCO in the pyrolysis of bark pellets. Both observations suggest pyrolysis-like production acting on polyamide-like material such as protein. The rate constant for the reaction of HNCO with OH at 298K is approximately 10^{-15} cm^3 molecule^{-1} s^{-1} as extrapolated from previous measurements [*Tsang*, 1992]. The ultraviolet absorption spectrum of isocyanic acid had been measured previously [*Dixon and Kirby*, 1968]. HNCO has a weak absorption in the ultraviolet suggesting that photolysis rates are most likely negligible when compared to hydrolysis, water uptake, and atmospheric transport. Atmospheric monitoring of this species combined with measurement of both Henry's coefficient and hydrolysis rate versus temperature are necessary to better understand the atmospheric fate of HNCO.

[43] Both formic and HONO emission ratios have been previously reported from field and laboratory studies. Figure 8 shows formic acid ER measurements from various laboratory and field experiments that emphasized sampling fresh smoke. There is significant scatter in ER measurements for both the laboratory and field data that have been published
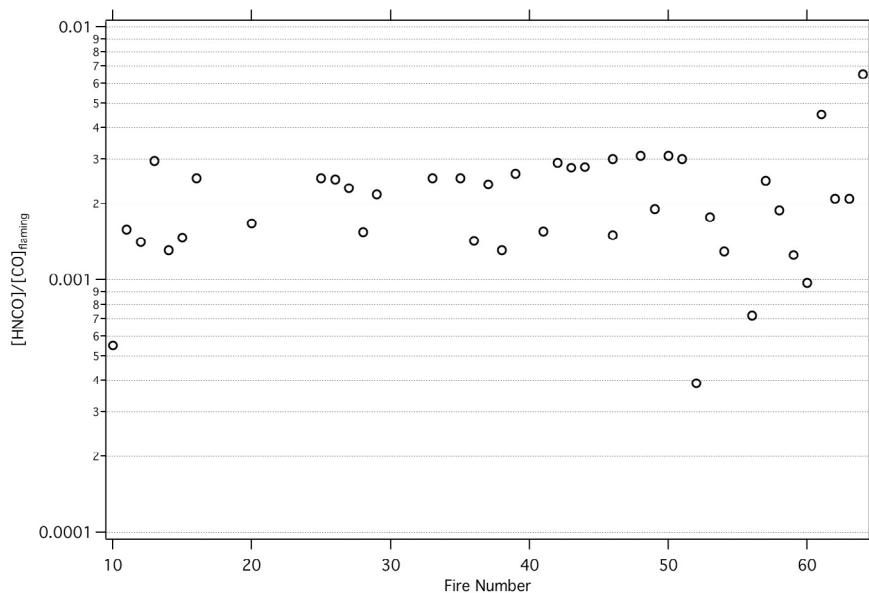
Figure 9. Summary of the ratio of HNCO measurements to CO produced by flaming for all of the fire samples. HNCO was emitted in a relatively constant ER in all of the fuel types sampled.

for formic acid. The relative plume age of the field measurements of smoke only minutes old has not been taken into account for the data reported. The scatter in initial ER from the laboratory studies makes any generalized comments on the fast photochemical production or loss of formic acid with plume age difficult on the time scale of minutes. On the time scale of hours secondary production of formic acid has been observed in Alaska [*Goode et al.*, 2000] and Brazil [*Yokelson et al.*, 2007a].

[44] Comparison of HONO emission ratios measured in this study to previous laboratory and field-measured emis-sion factors are shown in Figure 8. A lack of regional ER dependence is observed in these data. Several studies have proposed mechanisms for the heterogeneous production of HONO on surfaces [*Kleffmann et al.*, 1998], on humic aerosols [*Stemmler et al.*, 2007], aqueous aerosols [*Nienow and Roberts*, 2006], and black carbon [*Kalberer et al.*, 1999]. Thus in addition to the high amounts of HONO in fresh smoke that we have observed in these lab fires secondary production of additional HONO in the plume is also an important possibility. The presence of HONO in freshly emitted biomass burning plumes is significant, as HONO
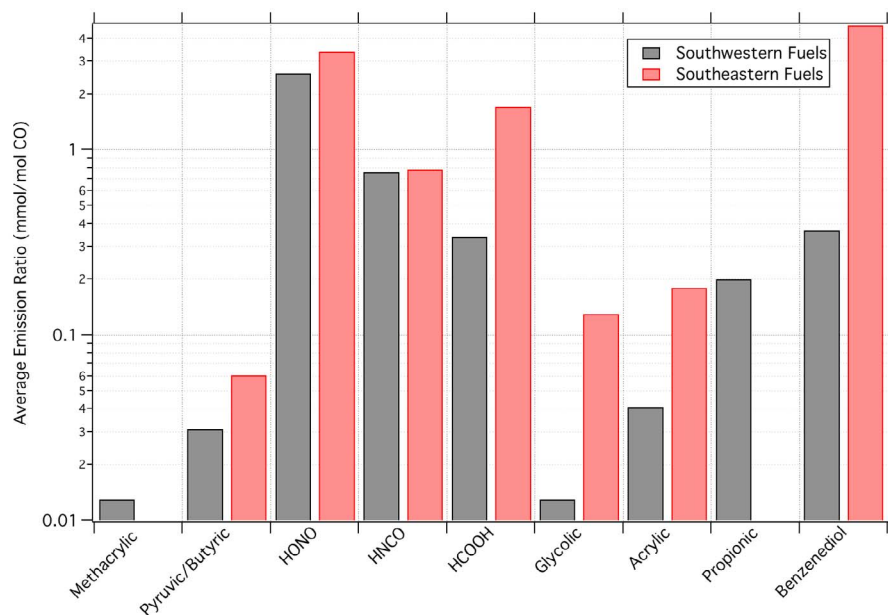

Figure 10. Summary of emission ratios for the nine compounds measured in this study. No data were collected for methacrylic and propionic acid in the southeastern fuels sampled.

Table 4. Summary of Molar Emission Ratios Relative to CO (ER$_{CO}$)[a]

Analyte	Southwest Fuels										Southeast Fuels							
	Ceanothus	Manzanita	CA Sage	Coastal Sage	Maritime Chaparral	Oak Savanna	Oak Woodland	Mesquite	Average	SD	1 yr Rough	2 yr rough	Treated NC	Pine Litter	Untreated NC	Pecosin	Average	SD
Methacrylic	0.013	-	-	-	-	-	-	-	0.013	-	-	-	-	-	-	-	-	-
Pyruvic/Butyric	-	0.010	0.091	0.048	0.018	0.014	0.014	0.020	0.031	0.029	0.038	0.096	0.005	0.010	0.047	0.080	0.061	0.037
HONO	2.0	1.8	2.0	4.6	2.1	3.9	4.1	2.3	2.6	0.95	4.6	4.0	2.2	1.2	4.3	4.1	3.4	1.4
HNCO	0.68	0.51	0.99	0.94	0.98	0.32	0.70	0.92	0.76	0.25	0.96	1.20	0.27	0.61	0.99	0.66	0.78	0.33
HCOOH	0.59	0.49	0.38	0.21	0.28	0.46	6.9E-03	0.34	0.34	0.18	1.4	2.3	8.3	1.9	1.2	2.4	1.7	0.63
Glycolic	0.016	0.014	0.011	0.002	0.0012	0.017	0.013	0.021	0.013	0.005	0.016	0.014	0.011	0.002	0.0012	0.017	0.013	0.021
Acrylic	0.065	0.033	0.025	0.018	0.037	0.042	0.081	0.024	0.041	0.022	0.21	0.27	0.33	0.22	0.13	0.21	0.18	0.08
Propionic	-	0.20	-	-	-	-	-	-	0.20	-	-	-	-	-	-	-	-	-
Benzenediol	-	-	0.20	0.09	0.42	0.25	0.73	0.50	0.37	0.23	6.7	5.6	5.8	5.6	2.4	1.9	4.7	2.0

[a]Units are (mmol Analyte emitted)(mol CO emitted)$^{-1}$. SD, standard deviation.

will readily photolyze to yield OH. Previous photochemical models have underestimated net ozone production in biomass plumes and the inclusion of additional HONO emissions in photochemical models of biomass plumes has been shown to increase the rate of initial plume chemistry [Alvarado and Prinn, 2009; Alvarado et al., 2009; Trentmann et al., 2005] and therefore help explain the observation of rapid O$_3$ formation in fresh biomass burning plumes.

[45] Table 4 shows a summary of organic acid emission ratios to CO for fuels from the two regions sampled. Figure 10 presents a comparison of emission ratios for fuels from the species measured in the two regions sampled. The sum of organic acids for the southwest is 3.2 μg m^{-3} ppmvCO^{-1} and the southeast total is 22.4 μg m^{-3} ppmvCO^{-1}. Benzenediol comprises 1.5 μg m^{-3} ppmvCO^{-1} to 18.0 μg m^{-3} ppmvCO^{-1} in the southwest and southeastern fuels, respectively. We can gain some insight into organic acid contribution to SOA formation by assuming a range of particulate yields from 17% to 86% as observed by Coeur-Tourneur et al. [2009] for the reaction of benzenediol with ozone measured under NO$_x$-free, low-relative humidity, and nonseeded conditions. That particular study concluded that either OH radical concentration is not significant or reaction of benzenediol with OH leads to similar yields as reaction with O$_3$. Using these aerosol yields, aerosol mass yields from 0.3 up to 15.5 μg m^{-3} ppmvCO^{-1} are possible from the reaction of benzenediol. de Gouw and Jimenez [2009] summarize organic aerosol total mass measured in various biomass burning emissions. Emission ratios of organic aerosols (OA) to CO observed in biomass smoke range from approximately 50 μg m^{-3} ppmvCO^{-1} up to 150 μg m^{-3} ppmvCO^{-1} at 295K and 1 atm. Using these reported emission ratios, the total contribution of benzenediol to organic aerosol mass can range from less than 1% to a maximum of 30%.

[46] Enhancement of organic acids in smoke plumes aged for several hours has been observed [Goode et al., 2000; Hobbs et al., 2003; Yokelson et al., 2009] and these secondary organic acids could be further oxidized to contribute to additional organic aerosol mass. The bulk of species measured in this study were not considered due to unavailability of aerosol yields. Thus, the total organic aerosol mass range that is reported here is considered a lower limit estimate. Measurements of particulate yields for all species in this study are necessary for a more detailed analysis of the organic acid contribution to total aerosol mass loadings.

5. Conclusions

[47] We used NI-PT-CIMS to measure the emissions of organic and inorganic acids from 34 laboratory biomass fires burning vegetation collected in the southeastern and southwestern United States. Formic acid and HONO emissions were measured and compared to previously published data. We also report emission ratios for isocyanic acid (HNCO), 1,2 and 1,3-benzenediols (catechol, resorcinol), acrylic acid, methacrylic acid, propionic acid, pyruvic acid, and glycolic acid measured from biomass burning.

[48] The comparison of simultaneous measurements of both formic acid and HONO from NI-PT-CIMS and OP-FTIR showed agreements within 20%. This work establishes NI-PT-CIMS as a valid real-time organic and inorganic acid measurement technique. The fast time response and low
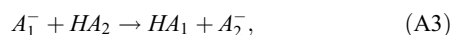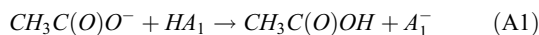
detection limits of this instrument provide the potential for in situ study of photochemical processing of fresh biomass smoke and for generalized measurements in urban air.

[49] We reported on the direct and very large release of HONO in biomass burning emissions that can have a significant impact on the initial rate of O_3 formation in biomass plumes. HNCO has been quantitatively observed for the first time in biomass emissions. The emission ratios presented are necessary to interpret field data and initiate models relevant to biomass plumes.

Appendix A: Ion Chemistry in the Flow Tube at High Mixing Ratios

[50] Even with inlet dilution, there were some occasions when high concentrations of analyte species required an assessment of the secondary chemistry occurring in the ion flow tube. In this section, we study if and how the removal of primary ions and the occurrence of secondary chemistry alter the calculation of mixing ratios according to equations (2)–(4). Equation (5) shows that the product ion concentration $[A^-]_t$ is linear in the organic acid concentration [HA]. While the dilution system shown in Figure 1 served to reduce primary ion loss, a significant reduction in the acetate ion signal was still observed in some cases. As a result, the approximation in equation (5) is no longer valid. In addition, secondary chemistry can become important when more than one organic acid is present at high mixing ratios, resulting in high concentrations of its conjugate anion.

[51] In this reduced reagent ion regime the following series of reactions can occur:

$$CH_3C(O)O^- + HA_1 \rightarrow CH_3C(O)OH + A_1^- \qquad (A1)$$

$$CH_3C(O)O^- + HA_2 \rightarrow CH_3C(O)OH + A_2^- \qquad (A2)$$

$$A_1^- + HA_2 \rightarrow HA_1 + A_2^-, \qquad (A3)$$

where HA_1 and HA_2 are two different acids with gas-phase acidities greater than acetic acid, and for which the gas-phase acidity of HA_2 is greater than that of HA_1. The solution for the above set of equations is investigated here to determine if it presents a significant problem in the data analysis that is typically used.

[52] To correct for secondary reactions, a numerical solution to the above equations was investigated in detail using:

$$[A_1^-]_t + \Delta t = [A_1^-]_t \times (1 - k_8[HA_2]_t \Delta t) + [CH_3C(O)O^-]_t \\ \times k_6[HA_1]\Delta t \qquad (A4)$$

$$[A_2^-]_t + \Delta t = [A_2^-]_t + [HA_2]_t \times \left(k_7[CH_3C(O)O^-]_t + k_8[A_1^-]_t\right)\Delta t \qquad (A5)$$

$$[CH_3C(O)O^-]_t + \Delta t = [CH_3C(O)O^-]_t(1 - k_6[HA_1]_t \Delta t) \\ - [CH_3C(O)O^-]_t k_7[HA_2]_t \Delta t, \qquad (A6)$$

where k_6, k_7, and k_8 are the reaction rates of equations (A1), (A2), and (A3), respectively, and Δt is the reaction time in

the flow tube 0.02 s. Two scenarios were investigated with assumed gas-phase acidities of $CH_3C(O)OH < HA_1 < HA_2$: (scenario I) large $[HA_2]$ significantly decreasing $[A_1^-]$ ions formed from reaction (A1), and (scenario II) large $[HA_1]$ forming additional ions that HA_2 can react with to form $[A_2^-]$.

[53] Initial model conditions were set such that $[CH_3C(O)O^-]_0 = 1$, $[A_1^-]_0 = 0$, and $[A_2^-]_0 = 0$, defined in terms of fractions of the initial $CH_3C(O)O^-$ concentration. The generated ions, $[A_1^-]_t$ and $[A_2^-]_t$, are then calculated as a fraction of the initial acetate ion concentration. The maximum concentration observed for a single species in a given fire was approximately 350 ppbv. Therefore, the model scenario uses a constant mixing ratio of 10 ppbv for the acid of interest after taking inlet dilution into account. Using these initial values, the two scenarios presented above were investigated.

[54] A value of 3.3×10^{-10} cm^3 $molecules^{-1}$ s^{-1} was calculated from the measured formic acid sensitivity for the rate coefficients of the proton-transfer reactions. The calculated rate coefficient is significantly less than the collision limit. One possible explanation is the presence of nonreactive acetate ion and water clusters that are dissociated upon exiting the flow tube.

[55] The results of this first-order approximation of the kinetics are shown in Figures A1a and A1b. In scenario I (Figure A1a), $[HA_2]$ was held constant at 10 ppbv while $[HA_1]$ was allowed to vary over several orders of magnitude. In scenario II (Figure A1b), $[HA_1]$ was held constant at 10 ppbv while $[HA_2]$ was varied. The relative ion signals (A_1^- and A_2^-) are not linear in the concentrations of organic acids (HA_2 and HA_1, respectively) as a result of primary ion depletion and secondary chemistry. This nonlinearity can be corrected for by normalizing to an effective primary ion signal. The results were used to determine the most effective normalization technique and quantify the corresponding error in the concentrations retrieved.

[56] Scenario I is presented in Figure A1a with a dashed line at 40 ppbv representing the sum of measured acids observed in a typical fire during this study. It is seen that the signal of acetate ions is significantly reduced under those conditions. The instrument response to A_2^- without normalization is depicted by the trace in red circles, and is relatively independent of $[HA_1]$. The trace shown in green diamonds shows the effect of the standard process of normalizing A_2^- to $CH_3C(O)O^-$. The normalized signal of A_2^- increases with $[HA_1]$, because of the removal of acetate ions. However, the A_1^- ions formed are also reactive with HA_2 and the trace in black triangles illustrates that normalizing to the sum of $CH_3C(O)O^-$ and A_1^- results in a signal for A_2^- that is independent of $[HA_1]$. We have shown here the simplified case of 2 organic acids at appreciable concentrations in the flow reactor. In the case where there are more than 2 species present, similar analyses show that the ion signal corresponding to an organic acid should be normalized to the signal of all ions from acids with a lesser gas-phase acidity.

[57] The second case investigated is the reaction of an acid HA_1 with $CH_3C(O)O^-$ by reaction (A1) and subsequent removal of the target ions, A_1^-, by reaction with additional reactive acids (HA_2) by reaction (A3). This case, Scenario II, is presented in Figure A1b. The measured signal of A_1^- ions (red circles) decreases significantly with HA_2, because of the decrease in acetate ions. Normalization to the sum of
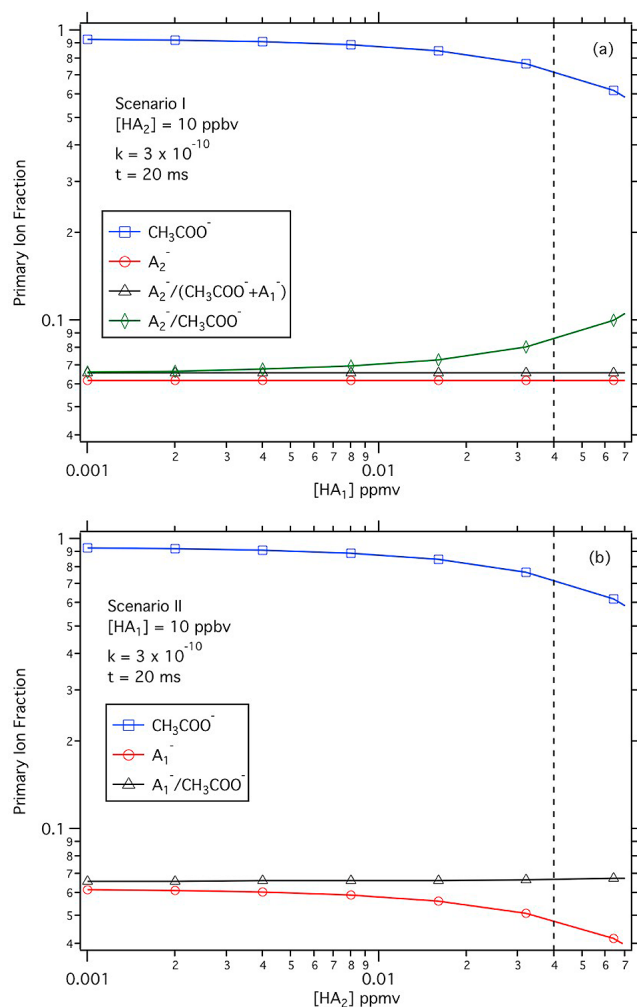
Figure A1. Kinetic model of the ion chemistry observed during this study. (a) Scenario I represents a situation in which two ions serve as proton acceptors for the acid of interest. (b) Scenario II illustrates a case in which the ion of interest becomes a proton acceptor for another acid present. The dashed line represents total concentration loadings at fire maximum as determined from measurements made during this study. Normalizing to ion signals, A_1^- and A_2^-, to the sum of ions that react with HA_1 or HA_2, respectively, to produce A_1^- and A_2^- effectively removes nonlinearities resulting from secondary chemistry.

ions that produce A_1^- (black triangles) results in constant signal through the concentrations observed at fire maximum. The resulting error observed by normalizing in this manner is <3%.

[58] In practice, measurements of a given acid were normalized to the sum of all measured ions that act as a proton acceptor. Based on this pseudo-first-order approximation of the reaction kinetics, less than a 3% error is associated with this normalization. It should be noted that a loss of primary ion signal of the magnitude observed during this study is unique to these high concentration fire emissions. Typical mixing ratios of reactive acids in the atmosphere are significantly lower than those measured in the fire plumes. As a

result, the data analysis used in this study is not necessary for most measurements made using NI-PT-CIMS.

References

Alvarado, M. J., and R. G. Prinn (2009), Formation of ozone and growth of aerosols in young smoke plumes from biomass burning: 1. Lagrangian parcel studies, *J. Geophys. Res.*, *114*, D09306, doi:10.1029/2008JD011144.

Alvarado, M. J., C. Wang, and R. G. Prinn (2009), Formation of ozone and growth of aerosols in young smoke plumes from biomass burning: 2. Three-dimensional Eulerian studies, *J. Geophys. Res.*, *114*, D09307, doi:10.1029/2008JD011186.

Amelynck, C., et al. (2000), Gas phase reactions of CF_3O^- and $CF_3O^-H_2O$ with nitric, formic, and acetic acid, *Int. J. Mass Spectrom.*, *203*(1–3), 165–175, doi:10.1016/S1387-3806(00)00321-3.

Burling, I. R., et al. (2010), Laboratory measurements of trace gas emissions from biomass burning of fuel types from the southeastern and southwestern United States, *Atmos. Chem. Phys. Discuss.*, *10*, 16,425–16,473, doi:10.5194/acpd-10-16425-2010.

Bytnerowicz, A., et al. (2009), *Wildland Fires and Air Pollution, Dev. Environ. Sci.*, vol. 8, 1st ed., 686 pp., Elsevier, Amsterdam.

Carlton, A. G., B. J. Turpin, H.-J. Lim, K. E. Altieri, and S. Seitzinger (2006), Link between isoprene and secondary organic aerosol (SOA): Pyruvic acid oxidation yields low volatility organic acids in clouds, *Geophys. Res. Lett.*, *33*, L06822, doi:10.1029/2005GL025374.

Christian, T. J., B. Kleiss, R. J. Yokelson, R. Holzinger, P. J. Crutzen, W. M. Hao, B. H. Saharjo, and D. E. Ward (2003), Comprehensive laboratory measurements of biomass-burning emissions: 1. Emissions from Indonesian, African, and other fuels, *J. Geophys. Res.*, *108*(D23), 4719, doi:10.1029/2003JD003704.

Christian, T. J., B. Kleiss, R. J. Yokelson, R. Holzinger, P. J. Crutzen, W. M. Hao, T. Shirai, and D. R. Blake (2004), Comprehensive laboratory measurements of biomass-burning emissions: 2. First intercomparison of open-path FTIR, PTR-MS, and GC-MS/FID/ECD, *J. Geophys. Res.*, *109*, D02311, doi:10.1029/2003JD003874.

Coeur-Tourneur, C., et al. (2009), Aerosol formation yields from the reaction of catechol with ozone, *Atmos. Environ.*, *43*(14), 2360–2365, doi:10.1016/j.atmosenv.2008.12.054.

Crutzen, P. J., and M. O. Andreae (1990), Biomass burning in the tropics—Impact on atmospheric chemistry and biogeochemical cycles, *Science*, *250*(4988), 1669–1678, doi:10.1126/science.250.4988.1669.

Custer, T. G., S. Kato, R. Fall, and V. M. Bierbaum (2000), Negative ion mass spectrometry and the detection of carbonyls and HCN front clover, *Geophys. Res. Lett.*, *27*(23), 3849–3852, doi:10.1029/2000GL011873.

de Gouw, J., and J. L. Jimenez (2009), Organic aerosols in the Earth's atmosphere, *Environ. Sci. Technol.*, *43*(20), 7614–7618, doi:10.1021/es9006004.

de Gouw, J. A., and C. Warneke (2007), Measurements of volatile organic compounds in the Earth's atmosphere using proton-transfer-reaction mass spectrometry, *Mass Spectrom. Rev.*, *26*(2), 223–257, doi:10.1002/mas.20119.

de Gouw, J. A., et al. (2005), Budget of organic carbon in a polluted atmosphere: Results from the New England Air Quality Study in 2002, *J. Geophys. Res.*, *110*, D16305, doi:10.1029/2004JD005623.

de Gouw, J. A., et al. (2006), Volatile organic compounds composition of merged and aged forest fire plumes from Alaska and western Canada, *J. Geophys. Res.*, *111*, D10303, doi:10.1029/2005JD006175.

Dixon, R. N., and G. H. Kirby (1968), Ultra-violet absorption spectrum of isocyanic acid, *Trans. Faraday Soc.*, *64*(548P), 2002, doi:10.1039/tf9686402002.

Goode, J. G., R. J. Yokelson, R. A. Susott, and D. E. Ward (1999), Trace gas emissions from laboratory biomass fires measured by open-path Fourier transform infrared spectroscopy: Fires in grass and surface fuels, *J. Geophys. Res.*, *104*(D17), 21,237–21,245, doi:10.1029/1999JD900360.

Goode, J. G., R. J. Yokelson, D. E. Ward, R. A. Susott, R. E. Babbitt, M. A. Davies, and W. M. Hao (2000), Measurements of excess O_3, CO_2, CO, CH4, C_2H_4, C_2H_2, HCN, NO, NH_3, HCOOH, CH_3COOH,

HCHO, and CH_3OH in 1997 Alaskan biomass burning plumes by airborne Fourier transform infrared spectroscopy (AFTIR), *J. Geophys. Res.*, *105*(D17), 22,147–22,166, doi:10.1029/2000JD900287.

Grieshop, A. P., et al. (2009), Laboratory investigation of photochemical oxidation of organic aerosol from wood fires. 1: Measurement and simulation of organic aerosol evolution, *Atmos. Chem. Phys.*, *9*(4), 1263–1277, doi:10.5194/acp-9-1263-2009.

Griffith, D. W. T. (1996), Synthetic calibration and quantitative analysis of gas-phase FT-IR spectra, *Appl. Spectrosc.*, *50*(1), 59–70, doi:10.1366/0003702963906627.

Hansson, K. M., et al. (2004), Formation of HNCO, HCN, and NH_3 from the pyrolysis of bark and nitrogen-containing model compounds, *Combust. Flame*, *137*(3), 265–277, doi:10.1016/j.combustflame.2004.01.005.

Hobbs, P. V., P. Sinha, R. J. Yokelson, T. J. Christian, D. R. Blake, S. Gao, T. W. Kirchstetter, T. Novakov, and P. Pilewskie (2003), Evolution of gases and particles from a savanna fire in South Africa, *J. Geophys. Res.*, *108*(D13), 8485, doi:10.1029/2002JD002352.

Huey, L. G. (2007), Measurement of trace atmospheric species by chemical ionization mass spectrometry: Speciation of reactive nitrogen and future directions, *Mass Spectrom. Rev.*, *26*(2), 166–184, doi:10.1002/mas.20118.

Kalberer, M., M. Ammann, F. Arens, H. W. Gäggeler, and U. Baltensperger (1999), Heterogeneous formation of nitrous acid (HONO) on soot aerosol particles, *J. Geophys. Res.*, *104*(D11), 13,825–13,832, doi:10.1029/1999JD900141.

Karl, T., A. Guenther, R. J. Yokelson, J. Greenberg, M. Potosnak, D. R. Blake, and P. Artaxo (2007), The tropical forest and fire emissions experiment: Emission, chemistry, and transport of biogenic volatile organic compounds in the lower atmosphere over Amazonia, *J. Geophys. Res.*, *112*, D18302, doi:10.1029/2007JD008539.

Keene, W. C., J. M. Lobert, P. J. Crutzen, J. R. Maben, D. H. Scharffe, T. Landmann, C. Hély, and C. Brain (2006), Emissions of major gaseous and particulate species during experimental burns of southern African biomass, *J. Geophys. Res.*, *111*, D04301, doi:10.1029/2005JD006319.

Kleffmann, J., et al. (1998), Heterogeneous NO_2 conversion processes on acid surfaces: Possible atmospheric implications, *Atmos. Environ.*, *32*(16), 2721–2729, doi:10.1016/S1352-2310(98)00065-X.

Linstrom, P. J., and W. G. Mallard (Eds.) (2010), NIST Chemistry WebBook, NIST Standard Ref. Database 69, http://webbook.nist.gov, Natl. Inst. of Stand. and Technol., Gaithersburg, Md.

McKenzie, L. M., et al. (1995), Measurement and modeling of air toxins from smoldering combustion of biomass, *Environ. Sci. Technol.*, *29*(8), 2047–2054, doi:10.1021/es00008a025.

McMeeking, G. R., et al. (2009), Emissions of trace gases and aerosols during the open combustion of biomass in the laboratory, *J. Geophys. Res.*, *114*, D19210, doi:10.1029/2009JD011836.

Mutch, R. W. (1994), Fighting fire with prescribed fire—A return to ecosystem health, *J. For.*, *92*(11), 31–33.

Nienow, A. M., and J. T. Roberts (2006), Heterogeneous chemistry of carbon aerosols, *Annu. Rev. Phys. Chem.*, *57*, 105–128, doi:10.1146/annurev.physchem.57.032905.104525.

Roberts, J. M., et al. (2010), Measurement of HONO, HNCO, and other inorganic acids by negative-ion proton-transfer chemical-ionization mass spectrometry (NI-PT-CIMS): Application to biomass burning emissions, *Atmos. Meas. Tech.*, *3*(4), 981–990, doi:10.5194/amt-3-981-2010.

Rothman, L. S., et al. (2009), The HITRAN 2008 molecular spectroscopic database, *J. Quant. Spectrosc. Radiat. Transfer*, *110*(9–10), 533–572, doi:10.1016/j.jqsrt.2009.02.013.

Stemmler, K., et al. (2007), Light induced conversion of nitrogen dioxide into nitrous acid on submicron humic acid aerosol, *Atmos. Chem. Phys.*, *7*(16), 4237–4248, doi:10.5194/acp-7-4237-2007.

Takegawa, N., et al. (2007), Contribution of selected dicarboxylic and omega-oxocarboxylic acids in ambient aerosol to the m/z 44 signal of an aerodyne aerosol mass spectrometer, *Aerosol Sci. Technol.*, *41*, 418–437, doi:10.1080/02786820701203215.

Trentmann, J., R. J. Yokelson, P. V. Hobbs, T. Winterrath, T. J. Christian, M. O. Andreae, and S. A. Mason (2005), An analysis of the chemical processes in the smoke plume from a savanna fire, *J. Geophys. Res.*, *110*, D12301, doi:10.1029/2004JD005628.

Tsang, W. (1992), Chemical kinetic data-base for propellant combustion - reactions involving CN, NCO, and HNCO, *J. Phys. Chem. Ref. Data*, *21*(4), 753–791, doi:10.1063/1.555914.

Veres, P., et al. (2008), Development of negative-ion proton-transfer chemical-ionization mass spectrometry (NI-PT-CIMS) for the measurement of gas-phase organic acids in the atmosphere, *Int. J. Mass Spectrom.*, *274*(1–3), 48–55, doi:10.1016/j.ijms.2008.04.032.

Veres, P., et al. (2010), Development and validation of a portable gas phase standard generation and calibration system for volatile organic compounds, *Atmos. Meas. Tech.*, *3*(3), 683–691, doi:10.5194/amt-3-683-2010.

Viggiano, A. A. (1993), In-situ mass-spectrometry and ion chemistry in the stratosphere and troposphere, *Mass Spectrom. Rev.*, *12*(2), 115–137, doi:10.1002/mas.1280120203.

Viidanoja, J., et al. (1998), Laboratory investigations of negative ion molecule reactions of formic and acetic acids: Implications for atmospheric measurements by ion-molecule reaction mass spectrometry, *Int. J. Mass Spectrom.*, *181*(1-3), 31–41, doi:10.1016/S1387-3806(98)14151-9.

Viidanoja, J., et al. (2000), Laboratory investigations of negative ion molecule reactions of propionic, butyric, glyoxylic, pyruvic, and pinonic acids, *Int. J. Mass Spectrom.*, *194*(1), 53–68, doi:10.1016/S1387-3806(99)00172-4.

Volkamer, R., J. L. Jimenez, F. San Martini, K. Dzepina, Q. Zhang, D. Salcedo, L. T. Molina, D. R. Worsnop, and M. J. Molina (2006), Secondary organic aerosol formation from anthropogenic air pollution: Rapid and higher than expected, *Geophys. Res. Lett.*, *33*, L17811, doi:10.1029/2006GL026899.

Walser, M. L., et al. (2007), Photochemical aging of secondary organic aerosol particles generated from the oxidation of d-limonene, *J. Phys. Chem. A*, *111*(10), 1907–1913, doi:10.1021/jp066293l.

Warneke, C., et al. (2009), Biomass burning in Siberia and Kazakhstan as the main source for Arctic haze over the Alaskan Arctic in April 2008, *Geophys. Res. Lett.*, *36*, L02813, doi:10.1029/2008GL036194.

Worden, H., R. Beer, and C. P. Rinsland (1997), Airborne infrared spectroscopy of 1994 western wildfires, *J. Geophys. Res.*, *102*(D1), 1287–1299, doi:10.1029/96JD02982.

Yokelson, R. J., D. W. T. Griffith, and D. E. Ward (1996), Open-path Fourier transform infrared studies of large-scale laboratory biomass fires, *J. Geophys. Res.*, *101*(D15), 21,067–21,080, doi:10.1029/96JD01800.

Yokelson, R. J., R. Susott, D. E. Ward, J. Reardon, and D. W. T. Griffith (1997), Emissions from smoldering combustion of biomass measured by open-path Fourier transform infrared spectroscopy, *J. Geophys. Res.*, *102*(D15), 18,865–18,877, doi:10.1029/97JD00852.

Yokelson, R. J., J. G. Goode, D. E. Ward, R. A. Susott, R. E. Babbitt, D. D. Wade, I. Bertschi, D. W. T. Griffith, and W. M. Hao (1999), Emissions of formaldehyde, acetic acid, methanol, and other trace gases from biomass fires in North Carolina measured by airborne Fourier transform infrared spectroscopy, *J. Geophys. Res.*, *104*(D23), 30,109–30,125, doi:10.1029/1999JD900817.

Yokelson, R. J., I. T. Bertschi, T. J. Christian, P. V. Hobbs, D. E. Ward, and W. M. Hao (2003), Trace gas measurements in nascent, aged, and cloud-processed smoke from African savanna fires by airborne Fourier transform infrared spectroscopy (AFTIR), *J. Geophys. Res.*, *108*(D13), 8478, doi:10.1029/2002JD002322.

Yokelson, R. J., et al. (2007a), The Tropical Forest and Fire Emissions Experiment: Overview and airborne fire emission factor measurements, *Atmos. Chem. Phys.*, *7*(19), 5175–5196, doi:10.5194/acp-7-5175-2007.

Yokelson, R. J., et al. (2007b), Emissions from forest fires near Mexico City, *Atmos. Chem. Phys.*, *7*(21), 5569–5584, doi:10.5194/acp-7-5569-2007.

Yokelson, R. J., et al. (2008), The tropical forest and fire emissions experiment: Laboratory fire measurements and synthesis of campaign data, *Atmos. Chem. Phys.*, *8*(13), 3509–3527, doi:10.5194/acp-8-3509-2008.

Yokelson, R. J., et al. (2009), Emissions from biomass burning in the Yucatan, *Atmos. Chem. Phys.*, *9*(15), 5785–5812, doi:10.5194/acp-9-5785-2009.

I. R. Burling and R. J. Yokelson, Department of Chemistry, University of Montana, Missoula, MT 59812, USA.

J. de Gouw, J. M. Roberts, P. Veres, and C. Warneke, Chemical Sciences Division, Earth System Research Laboratory, National Oceanic and Atmospheric Administration, 325 Broadway, Boulder, CO 80305, USA. (patrick.veres@noaa.gov)